The effect of force-field parameters on properties of liquids: Parametrization of a simple three-site model for methanol

Regula Walser, Alan E. Mark, and Wilfred F. van Gunsteren[a)]
Department of Physical Chemistry, Swiss Federal Institute of Technology Zürich, ETH-Zentrum, CH-8092 Zürich, Switzerland

Monika Lauterbach and Georges Wipff
Laboratoire MSM, Université Louis Pasteur, 4, rue Blaise Pascal, F-67000 Strasbourg, France

(Received 20 July 1999; accepted 8 March 2000)

A simple rigid three-site model for methanol compatible with the simple point charge (SPC) water and the GROMOS96 force field is parametrized and tested. The influence of different force-field parameters, such as the methanol geometry and the charge distribution on several properties calculated by molecular dynamics is investigated. In particular an attempt was made to obtain good agreement with experimental data for the static dielectric constant and the mixing enthalpy with water. The model is compared to other methanol models from the literature in terms of the ability to reproduce a range of experimental properties. © *2000 American Institute of Physics.* [S0021-9606(00)00921-1]

I. INTRODUCTION

Computer simulations are increasingly used to study and understand the properties of pure solvent mixtures and solute–solvent interactions at an atomic level. For example the properties of biomolecules such as proteins are strongly influenced by the nature of the surrounding solvent or solvent mixture.[1–6] To effectively study mixed systems it is a prerequisite that the models used to describe the individual components are compatible. That is, first they have to be derived in a consistent manner and second, they have to be parametrized not only to reproduce the properties of the isolated components but also of the mixture. Unfortunately, this is not always the case. A model for one compound parametrized to reproduce one set of properties may be combined with a model for another compound parametrized on a different set of properties and the interactions between the compounds derived using simple combination rules.

This paper describes the parametrization and testing of a simple rigid three-site model for methanol compatible with the simple point charge (SPC) water model[7] and the GROMOS96 force field.[8] The model is also compared to other methanol models from the literature including those proposed by Jorgensen[9] (referred to as J2), Haughney, Ferrario and McDonald[10,11] (referred to as H1) and van Leeuwen and Smit[12] (referred to as L1) in terms of the respective models ability to reproduce a wide range of experimental properties.

A number of simple models for methanol have been previously proposed. Jorgensen's OPLS model for methanol[9] (J2), based on an earlier TIP model,[13] was developed within a homologous series of alcohols by studying hydrogen-bonded methanol dimers and methanol–water complexes. The model was optimized to reproduce the heat of vaporization and the liquid density at ambient temperature and pressure based on Monte Carlo simulations in the NPT ensemble on a system of 128 methanol molecules using a cutoff of $R_c = 0.95$ nm and a correction term for Lennard-Jones interactions neglected beyond R_c. Amongst other properties investigated, the heat capacity and isothermal compressibility of his model agreed closely with experimental data.

Haughney *et al.*[10,11] developed two models for methanol (H1 and H2), as refinements of Jorgensen's TIP model,[13] designed primarily to better reproduce the strength of the hydrogen bonding. H1 differed from TIP only in the choice of charge distribution, while H2 differed also in the values used for the Lennard-Jones coefficients. They performed MD simulations based on the generalized methods of constraints[14] in the NVT ensemble for a system of 108 methanol molecules over a temperature range of approximately 80 K (260 K to 340 K) for their models H1 and H2 as well as for Jorgensen's OPLS and TIP models. Electrostatic interactions were treated by the Ewald method. They concluded that the models H1 and OPLS gave results for a range of properties, e.g., the self-diffusion coefficient, that overall are in good agreement with the available experimental data.

Stouten's model (OM2) was derived within a framework of a comparative research concerning hydrogen bonding in the crystalline and liquid phase of methanol.[15] Stouten performed MD simulations on a system of 216 methanol molecules at room temperature using a cutoff of 0.7 nm for the van der Waals interactions and of 1.1 nm for the Coulomb interactions, and obtained results comparable to those of Jorgensen's OPLS model[9] and the models of Haughney *et al.*[11] Stouten developed a second flexible model (OM1) for comparison with water concerning hydrogen bond properties.[15]

Van Leeuwen and Smit[12] re-refined the models of Jorgensen[9,13] and Haughney *et al.*[10,11] to reproduce phase coexistence properties of methanol over a wide range of temperatures (275 K to 525 K) and densities (up to 0.8 g cm^{-3}), based on studies of the vapor–liquid equilibria using Gibbs

a)Author to whom correspondence should be addressed. Electronic mail: wfvgn@igc.phys.chem.ethz.ch

ensemble Monte Carlo simulations.[16] This approach had previously been used by Mezei[17] to calculate the phase diagram for Jorgensen's OPLS model.[9]

In the current study we use a system of 512 molecules and long simulation times to expand the range of experimental properties previously used to compare the above models. The properties considered include: the heat of vaporization, the density at standard pressure, the diffusion constant, the viscosity, the dielectric constant, the isothermal compressibility, the heat capacity, the thermal expansion coefficient and the Debye relaxation time. We also investigate the sensitivity of a subset of these properties to changes in the van der Waals parameters, the partial charges assigned to the atoms, the geometry of the molecules, the effect of cutoff size and the effect of using a reaction field to treat the long-range Coulomb interactions.

Apart from the pure liquids, numerous studies of methanol–water binary mixtures are found in the literature. The solvation of a methanol molecule in water has been investigated by Monte Carlo simulation.[18–20] MD simulations of binary mixtures with different mole fractions of methanol are reported by Pálinkás *et al.*,[21,22] Stouten and Kroon,[23] Ferrario *et al.*,[24] Freitas,[25] and Laaksonen *et al.*[26] Wheeler and Rowley[27] have simulated ternary mixtures of water, methanol, and acetone. We present a comparison of the density and heat of mixing for a range of methanol–water concentrations to experimental values in order to demonstrate the compatibility of our chosen model B3 with the SPC water model. In addition, we calculate for the B3 model the excess Helmholtz energy and demonstrate that the model accurately reproduces the free energy of hydration of methanol in SPC water.

II. METHOD

All simulations were performed using the GROMOS96 simulation package.[8] The methanol was kept rigid by applying the SHAKE procedure[28] using a relative geometric accuracy of 10^{-4}. The intermolecular potential energy function was represented as the pairwise sum over all pairs of different molecules of a Coulomb and 12-6 Lennard-Jones interaction term,

$$U(r_{ij}) = \frac{C_{12}(i,j)}{r_{ij}^{12}} - \frac{C_6(i,j)}{r_{ij}^{6}} + \frac{q_i q_j}{4\pi\varepsilon_0 r_{ij}}, \tag{1}$$

where r_{ij} represents the distance between two atoms i and j, q_i the charge of atom i and ε_0 the dielectric permittivity of the vacuum. $C_6(i,j)$ and $C_{12}(i,j)$ are the Lennard-Jones coefficients for the interaction between atoms i and j. The potential energy $U(r_{ij})$ was calculated by using a twin-range cutoff. The nonbonded interaction between molecules, where the distance between their first atoms (oxygen atoms) lies within a spherical cutoff radius of $R_c = 0.9$ nm was calculated every step, while the interactions for molecules with distances between $R_c = 0.9$ nm and $R_{cl} = 1.4$ nm were evaluated only every fifth step. In the NVT simulations, the cubic periodic box with 3.2596 nm edge length contained 512 methanol molecules resulting in an experimental density[29] of 473.7 u nm^{-3}. During the NPT simulations the pressure was kept at 1 atm. The temperature (298 K) and pressure (NPT) were maintained by weak coupling to an external bath[30] using a coupling time of 0.1 ps for the temperature and 0.5 ps for the pressure. In the constant pressure runs, the isothermal compressibility of the system was set to 7.5×10^{-4} kJ^{-1} mol nm^3.

Where stated, a reaction-field term,[31,32] U_{RF}, was included in Eq. (1) to approximate the long-range Coulomb forces beyond R_{cl}, using a dielectric constant of the continuum[33] of $\varepsilon_{\mathrm{RF}} = 32.63$,

$$U_{\mathrm{RF}}(r_{ij}) = \frac{q_i q_j (\varepsilon_{\mathrm{RF}} - 1) r_{ij}^2}{4\pi\varepsilon_0 (2\varepsilon_{\mathrm{RF}} + 1) R_{cl}^3}. \tag{2}$$

A. Parametrization

The models were fitted to reproduce the experimental heat of vaporization ΔH_{vap} at a given temperature and pressure. The intermolecular potential energy can be related to the heat of vaporization by the expression,[34]

$$\Delta H_{\mathrm{vap}}(T) = -U(T) + p\Delta V + Q_{\mathrm{int}} + Q_{\mathrm{ext}}, \tag{3}$$

where ΔH_{vap} is the experimental molar heat of vaporization [ΔH_{vap} (298 K) = 37.99 kJ/mol],[29] U the intermolecular potential energy, p the pressure, and ΔV the molar volume change between liquid and gas ($p\Delta V$ is essentially equal to $pV_{\mathrm{gas}} = RT = 2.48$ kJ/mol at 298 K). The quantum correction term Q_{int} takes into consideration the difference in intramolecular vibrational energy between the liquid state and the gas phase and is approximately equal to 1.69 kJ/mol.[15] The second quantum correction term Q_{ext} applies only to liquids and depends on the active intermolecular vibrational modes. This term was taken equal to -1.81 kJ/mol.[15]

The methanol O–H bond length corresponded to the SPC water O–H distance,[15] while the starting O–Me bond lengths and the bond angle were based on structures obtained from microwave spectra.[35] The model M1a derived by Lauterbach[36] was chosen as a starting point for the parametrization procedure. Its parameters were derived from the GROMOS87 charge values and Lennard-Jones parameters for alcoholic oxygen (O), united atom CH_3 group (Me) and hydrogen (H).[37] The GROMOS force field does not contain a special hydrogen bonding term but mimics the effect of the hydrogen bonding properties of a polar atom such as an alcoholic oxygen by using different values for the van der Waals repulsion depending on the type of interaction. For nonhydrogen bonding pairs such as C_{12}(Me,O) the interaction is considered to be the geometrical mean of C_{12}^1(O,O) and C_{12}(Me,Me). For pairs of atoms involved in hydrogen bonds a second, larger value C_{12}^2(O,O) is used. The neglect of polarizability is counteracted by increasing the dipole above the experimental value in the gas phase. All models presented in Table I have a dipole between the experimental dipole in gas phase[33] of 1.7 D and the experimental dipole in liquid phase[38] of 2.9 D. For parametrization the charge of the hydrogen atom q_{H} was increased to 0.408 e, then the repulsive Lennard-Jones parameters C_{12} as well as the partial charge of the oxygen q_{O} were adjusted, so that the potential energy and the pressure during the MD simulations ap-

TABLE I. Geometries and charges of the presented models. Here q denotes the partial charges, d the distances between atoms of the molecule and μ the dipole of the molecule.

Model name	q_H (e)	q_O (e)	q_{Me} (e)	d_{OH} (nm)	d_{MeO} (nm)	d_{HMe} (nm)	μ (D)
GR96 (Refs. 8, 39)	0.398	−0.574	0.176	0.1000	0.1430	0.1988	1.91
H1 (Refs. 10, 11)	0.431	−0.728	0.297	0.0945	0.1425	0.1944	2.33
J2 (Ref. 9)	0.435	−0.700	0.265	0.0945	0.1430	0.1948	2.22
L1 (Ref. 12)	0.435	−0.700	0.265	0.0945	0.1424	0.1944	2.22
M1a (Ref. 36)	0.398	−0.574	0.176	0.1000	0.1430	0.1988	1.91
A1	0.408	−0.634	0.226	0.1000	0.1430	0.1988	2.08
A2	0.408	−0.654	0.246	0.1000	0.1430	0.1988	2.15
A3	0.408	−0.674	0.266	0.1000	0.1430	0.1988	2.22
B3	0.408	−0.674	0.266	0.1000	0.1530	0.2077	2.29

proached their target values of −35.6 kJ/mol, calculated from the heat of vaporization using Eq. (3), and 1 atm, respectively. The effect of increasing the dipole by extending the bond between the O- and the Me-atom d_{OMe} was also investigated. The attractive Lennard-Jones parameters were set to the GROMOS96 values,[8,39] and q_{Me} was set equal to $-q_O-q_H$ in order to preserve electro neutrality.

The parametrization simulations were 300 ps in length of which 50 ps was for equilibration. No reaction-field correction was applied and the simulations were performed at constant volume.

B. Properties

To study the influence of different force-field parameters on the properties of liquid methanol 4 different models were developed and compared. They are named A1, A2, A3, and B3, where the number refers to the charge distribution and the letter to the bond length of d_{OMe}. These models are also compared to other models taken from the literature. The literature models are referred to as GR96, for the MeOH model of the GROMOS96 force field,[8] H1 for the model of Haughney *et al.*,[10,11] J2 for the OPLS model of Jorgensen[9] and L1 for the model of van Leeuwen and Smit.[12] The geometries and charge distributions of these models are summarized in Table I and the Lennard-Jones interaction parameters in Table II.

For each model studied a 1 ns MD simulation with reaction-field correction at 298 K was performed. The last 900 ps of these simulations were used for analysis. Additional simulations with a different setup were performed where necessary.

1. Self-diffusion coefficient D

The diffusion coefficient was calculated from the mean-square displacement of the particles using the Einstein relation,

$$D=\lim_{t\to\infty}\frac{\langle(\mathbf{r}(t)-\mathbf{r}(0))^2\rangle}{6t}, \tag{4}$$

where $\mathbf{r}(t)$ denotes the position vector of a molecule at time t.

2. Shear viscosity η

The viscosity was calculated as described by Tironi and van Gunsteren.[40] The off-diagonal elements P_{xy}, P_{xz}, P_{yz} of the pressure tensor[41] are given by

$$P_{\alpha\beta}(t)=\frac{1}{V}\left(\sum_i \frac{p_{\alpha i}(t)p_{\beta i}(t)}{m_i}+\sum_{i<j} F_{\alpha ij}(t)\beta_{ij}(t)\right), \tag{5}$$

where α and β denote x, y or z components of the interparticle vector $\mathbf{r}_{ij}\equiv\mathbf{r}_i-\mathbf{r}_j$, $p_{\alpha i}$ the α-component of the momentum of particle i and $F_{\alpha ij}$ the α-component of the force exerted on particle i by particle j. The shear viscosity η has been calculated from the displacement of $P_{\alpha\beta}$:

TABLE II. The Lennard-Jones interaction parameters for the different methanol models. $(C_{6,12}(\mathrm{I}))^{1/2}$ are the single atom van der Waals parameters for atom I. $(C^1_{12}(\mathrm{O}))^{1/2}$ is used for combinations with Me, while $(C^2_{12}(\mathrm{O}))^{1/2}$ is used for interactions with O atoms.

Model name	$(C^1_{12}(\mathrm{O}))^{1/2}$ $10^{-3}\left(\frac{\mathrm{kJ\,mol}}{\mathrm{nm}^{12}}\right)^{1/2}$	$(C^2_{12}(\mathrm{O}))^{1/2}$ $10^{-3}\left(\frac{\mathrm{kJ\,mol}}{\mathrm{nm}^{12}}\right)^{1/2}$	$(C_{12}(\mathrm{Me}))^{1/2}$ $10^{-3}\left(\frac{\mathrm{kJ\,mol}}{\mathrm{nm}^{12}}\right)^{1/2}$	$(C^1_6(\mathrm{O}))^{1/2}$ $\left(\frac{\mathrm{kJ\,mol}}{\mathrm{nm}^{6}}\right)^{1/2}$	$(C^2_6(\mathrm{O}))^{1/2}$ $\left(\frac{\mathrm{kJ\,mol}}{\mathrm{nm}^{6}}\right)^{1/2}$	$(C_6(\mathrm{Me}))^{1/2}$ $\left(\frac{\mathrm{kJ\,mol}}{\mathrm{nm}^{6}}\right)^{1/2}$
GR96 (Refs. 8, 39)	1.1250	1.227	4.5665	0.0476	0.0476	0.0942
H1 (Refs. 10, 11)	1.5839	1.4683	5.7685	0.0521	0.0501	0.1002
J2 (Ref. 9)	1.4124	1.4124	5.3864	0.0488	0.0488	0.1001
L1 (Ref. 12)	1.3126	1.3126	5.1191	0.0472	0.0472	0.0979
M1a (Ref. 36)	1.1247	1.2272	4.5665	0.0476	0.0476	0.0942
A1	1.3250	1.3970	4.5665	0.0476	0.0476	0.0942
A2	1.3250	1.4450	4.5665	0.0476	0.0476	0.0942
A3	1.5250	1.4570	4.5665	0.0476	0.0476	0.0942
B3	1.5250	1.5250	4.400	0.0476	0.0476	0.0942

$$\Delta P_{\alpha\beta}(t)=\int_0^t P_{\alpha\beta}(t')dt' \tag{6}$$

via the Einstein relation

$$\eta=\frac{1}{2}\frac{V}{k_BT}\lim_{t\to\infty}\frac{d}{dt}\langle\Delta P_{\alpha\beta}^2(t)\rangle. \tag{7}$$

Because of poor statistics at long times only $\langle\Delta P_{\alpha\beta}^2(t)\rangle$ between 5 ps and 10 ps was used for analysis.

3. Dielectric constant ε_S

For most purposes the frequency-dependent relative (i.e., with respect to the vacuum value ε_0) dielectric permittivity $\varepsilon(\omega)$ can be modeled by the Debye equation

$$\varepsilon(\omega)=\varepsilon(\infty)+\frac{\varepsilon(0)-\varepsilon(\infty)}{(1+i\omega\tau_D)^p}, \tag{8}$$

where τ_D is the Debye relaxation time defined in (11) below, and p adopts values close to one, e.g., $p=0.986$ for water. The infinite-frequency value $\varepsilon_\infty=\varepsilon(\infty)$ is due to displacements of electrons and the zero frequency or static value $\varepsilon_S=\varepsilon(0)$ is due to dipolar orientation. The relative static dielectric constant for methanol was calculated from the fluctuations of the total dipole moment $\mathbf{M}$ of the system, using the formula of Neumann:[42]

$$(\varepsilon_S-1)\frac{2\varepsilon_{\mathrm{RF}}+1}{2\varepsilon_{\mathrm{RF}}+\varepsilon_S}=\frac{\langle\mathbf{M}^2\rangle-\langle\mathbf{M}\rangle^2}{3\varepsilon_0 Vk_BT}, \tag{9}$$

where $\varepsilon_{\mathrm{RF}}$ is the relative dielectric constant of the continuum employed in the reaction-field term in Eq. (2). To avoid the suppression of the fluctuations in the total dipole moment caused by the application of an electrostatic interaction cutoff, all simulations used to determine the dielectric constant were performed using a reaction field.

4. Debye relaxation time τ_D

The Debye relaxation time τ_D was calculated from the autocorrelation function $\Phi(t)$ of the total dipole moment $\mathbf{M}$ of the box which can be fitted to an exponential decay:

$$\Phi(t)=\frac{\langle\mathbf{M}(t)\mathbf{M}(0)\rangle}{\langle M^2(0)\rangle}=e^{-(t/\tau_\Phi)} \tag{10}$$

via[31]

$$\tau_D=\frac{2\varepsilon_{\mathrm{RF}}+\varepsilon_S}{2\varepsilon_{\mathrm{RF}}+1}\tau_\Phi. \tag{11}$$

5. Isothermal compressibility κ_T

The isothermal compressibility can be estimated from the following expression,[43] relating two state points 1 and 2:

$$\kappa_T=-\frac{1}{V}\left(\frac{\partial V}{\partial p}\right)_T=\frac{1}{\rho}\left(\frac{\partial\rho}{\partial p}\right)_T=\left(\frac{\partial\ln(\rho)}{\partial p}\right)_T\approx\left(\frac{\ln\left(\frac{\rho_2}{\rho_1}\right)}{p_2-p_1}\right)_T, \tag{12}$$

where ρ is the density of the system.

To calculate the compressibility, an additional simulation with a decreased volume of 33.233 nm^3 was performed.

6. Thermal expansion coefficient α

A similar finite difference expression for the thermal expansion coefficient is[40]

$$\alpha=\frac{1}{V}\left(\frac{\partial V}{\partial T}\right)_p\approx-\left(\frac{\ln\left(\frac{\rho_2}{\rho_1}\right)}{T_2-T_1}\right)_p. \tag{13}$$

To calculate α two simulations were performed at constant pressure, one at 298 K and one at 328 K.

7. Heat capacity C_p

The constant volume heat capacity was obtained using the following equation:[40]

$$C_V=\left(\frac{\partial E}{\partial T}\right)_V\approx\left(\frac{U_2-U_1}{T_2-T_1}\right)_V+3R+C_V^{\mathrm{vib}}, \tag{14}$$

where E is the total and U the potential energy. C_V^{vib} is a correction term for the vibrational contribution to the heat capacity when comparing the rigid methanol model of the simulation to experiment. It can be estimated from the partition function for a harmonic quantum-mechanical oscillator using experimental normal mode frequencies.[44] Using values from Herzberg[44] and Wilson,[45] it was calculated as 5.749 $\mathrm{J\,mol^{-1}\,K^{-1}}$. The constant pressure heat capacity C_P can then be calculated from C_V using the following relation:[46]

$$C_P-C_V=T\frac{v\alpha^2}{\kappa_T}, \tag{15}$$

where v is the molar volume, α the thermal expansion coefficient, and κ_T the isothermal compressibility.

8. Binary mixtures

A certain number out of 1000 methanol molecules was replaced by SPC water molecules[7] to obtain binary mixtures with the desired mole fraction of methanol x_{MeOH}. Simulations with x_{MeOH} of 0.000, 0.125, 0.250, 0.375, 0.500, 0.625, 0.750, 0.875, and 1.000 were performed at constant pressure without a reaction-field correction. Each mixture was simulated for 1 ns, only the last 900 ps were used for analysis.

The molar enthalpy of mixing was calculated from the potential energy via

$$\Delta H_{\mathrm{mix}}=U(\mathrm{mix})-x_{\mathrm{MeOH}}U(\mathrm{MeOH})-(1-x_{\mathrm{MeOH}})U(\mathrm{H_2O}), \tag{16}$$

where $U(\mathrm{mix})$ is the potential energy of the mixture and $U(\mathrm{MeOH})$ and $U(\mathrm{H_2O})$ the potential energy of pure methanol and pure water, respectively.

9. Free energy

The free energy differences between two states A and B can be expressed as

TABLE III. The effect of increasing the dipole moment by changing the charge distribution is shown. Here p denotes the pressure, U the potential energy, D the self-diffusion coefficient, ε_S the static permittivity and τ_D the Debye relaxation time. The other parameters are the same as in Table I. The experimental values are at 298 K and 1 atm, except ε_S, which is at 293 K.

Model name	q_H (e)	q_O (e)	q_{Me} (e)	μ (D)	p $\left(\frac{\text{kJ}}{\text{mol nm}^3}\right)$	U $\left(\frac{\text{kJ}}{\text{mol}}\right)$	D $\left(10^{-3}\ \frac{\text{nm}^2}{\text{ps}}\right)$	ε_S	τ_D (ps)
A1	0.408	−0.634	0.226	2.08	−8.060	−35.5	2.9	21.3	33
A2	0.408	−0.654	0.246	2.15	−11.035	−35.5	2.9	24.3	32
A3	0.408	−0.674	0.266	2.22	0.283	−35.5	2.6	20.2	25
Expt.				1.7 (Ref.33)	0.061	−35.6	2.4 (Ref.65)	32.6 (Ref.33)	49 (Ref. 54)

$$\Delta F_{BA} = \int_{\lambda_A}^{\lambda_B} F'(\lambda)\, d\lambda = \int_{\lambda_A}^{\lambda_B} \left\langle \frac{\partial H}{\partial \lambda} \right\rangle d\lambda, \tag{17}$$

where the Hamiltonian H has been made dependent on a coupling parameter λ and the angular brackets $\langle\ \rangle$ denote averaging over an equilibrium ensemble generated with $H(\lambda)$. The integral in Eq. (17) was evaluated by obtaining ensemble averages at 25 discrete λ points and determining the integral numerically. At each λ point 20 ps equilibration and 50 ps samplings were performed. To avoid numerical instabilities as atoms were created or deleted a soft-core interaction function[47,48] was used as described by Daura *et al.*[49]

The excess Helmholtz energy was obtained by changing the liquid state ($\lambda=0$) to the gas state ($\lambda=1$) by switching off the nonbonded interactions in a NVT simulation.[40,50] It is compared to an experimental value of 17.9 $\text{kJ mol}^{-1}\,\text{K}^{-1}$ calculated by

$$\Delta A \approx RT\left(\ln\left(\frac{RT}{p_{\text{vap}} v}\right) - 1\right), \tag{18}$$

where p_{vap} is the vapor pressure at temperature T and v the molar volume of the solvent. For methanol at 298 K p_{vap} is[29] $0.164\times10^{-25}\text{kJ/nm}^3$.

The hydration free energy was calculated by growing a methanol molecule in a box of 999 SPC water molecules. This was done by turning on the nonbonded interactions of this molecule to the water molecules. The pressure was kept constant.

III. EFFECT OF THE PARAMETERS

The influence of different force-field parameters and simulation conditions on the simulated properties was investigated. The force-field parameters investigated include the charge distribution and the geometry of the methanol model. By adjusting the Lennard-Jones parameters it was possible to get agreement with the experimental values for the pressure and the potential energy for all tested models. That the models reproduce pressure and potential energy does not necessarily mean that other properties are also well reproduced. Especially the dielectric properties may deviate from the experimental value. We therefore calculated the dielectric constant and the Debye relaxation time for the different models, to examine how they depend on the geometry and charge distribution and if there exists a simple relationship between these parameters and the calculated results. Not only the model parameters, but also the exact simulation conditions influence the results of the calculation of the properties. Therefore the influence of simulating at constant pressure versus constant volume as well as different treatment of the long-range interaction forces, i.e., long-range cutoff and inclusion of a reaction-field force was also examined.

A. Charge distribution

The results of increasing the dipole moment by changing the charge distribution are summarized in Table III. The target value for the potential energy U was reached, while the value for the pressure p, which is more sensitive to the exact simulation conditions, differs more from the experimental value. By gradually increasing the dipole moment μ of the methanol model a slight decrease of the diffusion constant D was obtained, but it seems to be rather insensitive to the dipole moment of the molecule. The permittivity ε_S did not show a consistent trend and differed in all models by about 50% from the experimental value. The Debye relaxation time decreased as a function of the dipole moment.

B. Bond length

Since increasing the dipole moment by changing the charge distribution did not result in a permittivity closer to the experimental value, the dipole moment was increased by increasing the Me–O bond. An increase of the bond length may be justified when it is considered that the center of mass of the Me group lies not on the C atom but is shifted 0.0073 nm outwards. This is a very small length increase, which does not increase the simulated permittivity significantly. A larger but still small bond length increase of 0.036 nm is obtained by considering the center of geometry of the H atoms of the Me group. However, to obtain a significant increase of the simulated permittivity, the Me–O bond was increased by 0.1 nm to the value of a CH_n–CH_n bond. We note that when using a united-atom representation, i.e., implicit aliphatic hydrogen atoms, model parameters such as the united-atom bond lengths, bond angles, and charge distribution are nonphysical quantities, whose values cannot be expected to have a physical meaning and should therefore not be compared to experimental values. The effect of changing the Me–O bond length is shown in Table IV. Though the

TABLE IV. The effect of increasing the dipole by enlarging the Me–O bond length. The symbols are the same as in Tables I and III.

Model name	d_{OH} (nm)	d_{MeO} (nm)	d_{HMe} (nm)	μ (D)	p $\left(\frac{\text{kJ}}{\text{mol nm}^3}\right)$	U $\left(\frac{\text{kJ}}{\text{mol}}\right)$	D $\left(10^{-3}\ \frac{\text{nm}^2}{\text{ps}}\right)$	ε_S	τ_D (ps)
A3	0.100	0.143	0.199	2.22	0.283	−35.5	2.6	20.2	25
B3	0.100	0.153	0.208	2.29	0.523	−35.3	2.6	22.7	17
Expt.				1.7 (Ref.33)	0.061	−35.6 (Ref.33)	2.4 (Ref.65)	32.6 (Ref.33)	49 (Ref. 54)

permittivity is increased it still remains far from the experimental value. The diffusion is not affected by the change, while the Debye relaxation time shortens.

Comparing these results to that of two water models SPC[7] and SPC/E,[51] where an increase in the dipole moment of only 3% from 2.28 D to 2.35 D leads to an increase in the permittivity of 15% from 54.0 to 62.3,[52] one sees that increasing the dipole moment is much less effective for the methanol models. The dipole increases from model A1 to B3 by 10%, but the permittivity increases only by 6%. The most likely reason for this is related to the fact that we are considering only nonpolarizable models. **M** can be considered to be composed of two contributions $\mathbf{M}_l$ and $\mathbf{M}_h$, referring to low and high frequency components, respectively. For dipolar substances $\mathbf{M}_h$ is mainly due to the displacement of the electrons and $\mathbf{M}_l$ to the orientation of the dipoles. For nonpolarizable models **M** is in effect assumed equal to $\mathbf{M}_l$. $\mathbf{M}_l$ can be expressed as[53]

$$\frac{M_l^2}{3\varepsilon_0 V k_B T} = \frac{(\varepsilon_S - \varepsilon_\infty)(2\varepsilon_{RF}+1)^2}{(2\varepsilon_{RF}+\varepsilon_\infty)(2\varepsilon_{RF}+\varepsilon_S)}, \tag{19}$$

thus only if $\varepsilon_\infty = 1$ is $\mathbf{M}_l$ truly equal to **M**. The greater ε_∞ becomes in comparison to ε_S the more will $\mathbf{M}_l$ differ from **M**. For water ε_∞ and ε_S are[33] 5.2 and 78.4, respectively, while for methanol the experimental values are[54,33] 5.38 and 32.63, respectively. Therefore, it is to be expected that the permittivity of water can be better reproduced by an unpolarizable model than is the case for methanol.

We note that since the GROMOS96 force field[8] does not include explicit polarizability and has been parametrized without taking into account the self-polarization energy of dipoles, it is more consistent with the SPC water model,[7] which has also omitted the self-polarization term, than with the SPC/E water model,[51] which has been parametrized including self-polarization. Since our goal is to derive a simple rigid three-site model for methanol compatible with the SPC water model and the GROMOS96 force field, we did not include a self-polarization energy term when fitting the energy of liquid methanol to the experimental heat of vaporization.

C. Treatment of long-range forces

The effects of different treatment of the long-range forces are summarized in Table V. Two different aspects are considered, one is the inclusion of a long-range cutoff, and the other the use of a reaction-field contribution to the forces due to the dielectric continuum beyond the outer cutoff. The inclusion of a reaction-field contribution changes the pressure by a factor of about 10 if it is applied outside a long-range cutoff R_{cl} of 1.4 nm (model B3) and even more if only a single cutoff R_c of 0.9 nm is used (model M1a). Inclusion of long-range forces between $R_c = 0.9$ nm and $R_{cl} = 1.4$ nm also affects the pressure (model H1). The potential energy is hardly affected by the addition of a reaction-field force. The change is greater but still small when a long-range cutoff is used. The permittivity is not very sensitive to the long-range cutoff used.

D. Constant volume versus constant pressure

Analyzing the different simulations we found differences in the permittivity between the simulations done at constant

TABLE V. The effect of different treatment of the long-range interactions. R_{cl} is the long-range cutoff, RF and no RF mean that the simulations have been done with and without a reaction-field contribution to the forces, respectively.

Model name	R_{cl}[a] (nm)	Reaction field	p $\left(\frac{\text{kJ}}{\text{mol nm}^3}\right)$	U $\left(\frac{\text{kJ}}{\text{mol}}\right)$	D $\left(10^{-3}\ \frac{\text{nm}^2}{ps}\right)$	ε_S
B3	1.4	no RF	0.065	−35.2	2.4	
B3	1.4	RF	0.523	−35.3	2.6	22.7
H1 (Refs. 10, 11)	0.9	RF	61.038	−34.7		20.6
H1 (Refs. 10, 11)	1.4	RF	86.619	−34.0		20.4
M1a[b]	0.9	no RF	0.122	−35.5	3.1	
M1a[b]	0.9	RF	4.393	−35.3		
M1a[b]	1.5	no RF	−21.356	−36.2		

[a]In all simulations $R_c = 0.9$ nm.
[b]The results for model M1a are taken from Lauterbach (Ref. 36).

TABLE VI. Simulating at constant pressure or volume may influence the calculated dielectric permittivity. In the table ρ denotes the density of the system, the other symbols are the same as in Tables I and III.

Model name	Simulation time (ns)		p $\left(\frac{\text{kJ}}{\text{mol nm}^3}\right)$	ρ $\left(\frac{\text{u}}{\text{nm}^3}\right)$	U $\left(\frac{\text{kJ}}{\text{mol}}\right)$	D $\left(10^{-3}\ \frac{\text{nm}^2}{\text{ps}}\right)$	ε_S	τ_D (ps)
A2	1	NVT	−11.035	473.70	−35.496	2.9	24.3	32
		NPT	0.051	486.35	−35.877	2.4	19.0	25
B3	1	NVT	0.523	473.70	−35.349	2.6	22.7	17
		NPT	0.051	473.07	−35.351	2.3	18.6	14
B3	2	NVT	0.907	473.70	−35.348	2.6	22.7	17
		NPT	0.048	473.23	−35.350	2.4	19.8	14

pressure and those at constant volume. The results for the two models simulated at both conditions are summarized in Table VI. While it might be possible that the differences for model A2 arise from the pressure difference between the two simulations, this is not the case for model B3, where the pressure differs only slightly. Another possibility is that the permittivity has not yet converged. The two runs of B3 were therefore continued for a further 1 ns. While the permittivity obtained from the constant pressure run approaches the result of the constant volume run, the difference is still considerable. Given a sufficiently large system the two ensembles are equivalent. Since only the value of the simulation at constant pressure changed when increasing the simulation length, the permittivity probably is converged after 1 ns when simulated at constant volume but takes longer to converge when simulating at constant pressure.

IV. PROPERTIES OF MODEL B3

The model B3 showed the best overall agreement with experimental values. Therefore, it was evaluated further and compared to other models from the literature (see Table VII). The model was parametrized to reproduce the pressure and potential energy and therefore the calculated values are close to the experimental values. All the other models show large deviations in the pressure. The L1 model comes closest to the experimental value, while the H1 model deviates the most. This is consistent with the results of Haughney *et al.*[11] who reported a pressure of about 47 $\text{kJ mol}^{-1}\,\text{nm}^{-3}$ at 299.3 K. In the simulations at constant pressure the density of the model J2 differs from the experimental value by almost 5%. L1 having too high of a value for the pressure is in contrast with the results of Mountain,[55] who obtained a negative pressure when simulating at experimental density at 288 K. It is important to note that the calculated pressure is very sensitive to the method of simulation, the size of the system and the effective cutoff radius[15] (see also Table V). The model J2 was parametrized using a correction term for the Lennard-Jones interactions neglected beyond the cutoff distance of 0.95 nm. In contrast, Haughney *et al.*[11] used Ewald summation for the electrostatic interactions when developing the model H1 (and H2) and comparing to Jorgensen's model J2 (and J1). Such differences in methodology most likely explain the discrepancies between the values shown in table VII and the equivalent values of Haughney *et al.*[11] or by Stouten.[15] Each model would be expected to perform best under the conditions it was parametrized. However, as the current aim is to develop a methanol model compatible with the SPC water model[7] and protein force fields,[8,39] we restrict ourselves to treating the long-range interactions by applying cutoffs and reaction-field contributions.

A. Transport properties

The diffusion coefficient for model B3 is too high compared to the experimental value. In contrast, the diffusion coefficient of model H1 is of about the same difference too low, possibly as a result of the too high pressure. The result for model L1 is even lower than for model H1 and agrees with the result of Mountain,[55] who got $1.8\times10^{-3}\ \text{nm}^2\,\text{ps}^{-1}$ at a lower temperature of 288 K. The values for models H1 and J2 are higher than those of Haughney *et al.*[11] or Asahi and Nakamura.[56] Haughney *et al.* pointed out in their paper that a large diffusion coefficient might be expected for a model that underestimates the strength of hydrogen bonding in the liquid. Large diffusion coefficients are also commonly

TABLE VII. Comparison to other models from the literature. The model names are the same as used in the text.

	Model name	μ (D)	p $\left(\frac{\text{kJ}}{\text{mol nm}^3}\right)$	ρ $\left(\frac{\text{u}}{\text{nm}^3}\right)$	U $\left(\frac{\text{kJ}}{\text{mol}}\right)$	D $\left(10^{-3}\ \frac{\text{nm}^2}{\text{ps}}\right)$	ε_S	τ_D (ps)
NVT	GR96	1.9	−21.872	473.7	−36.1	3.1	17.7	19
	H1 (Refs. 10, 11)	2.33	61.038	473.7	−34.7	2.2	20.6	16
	L1 (Ref. 12)	2.22	2.203	473.7	−37.6	1.9	18.1	33
	B3	2.29	0.523	473.7	−35.3	2.6	22.7	17
NPT	J2 (Ref. 9)	2.22	0.094	453.7	−35.3	2.6	21.0	18
	B3	2.29	0.05	473.1	−35.4	2.3	18.6	14

TABLE VIII. Properties of model B3 obtained at different temperatures.

	298 K				328 K			
	p $\left(\frac{\text{kJ}}{\text{mol nm}^3}\right)$	ρ $\left(\frac{\text{u}}{\text{nm}^3}\right)$	D $\left(10^{-3}\ \frac{\text{nm}^2}{\text{ps}}\right)$	ε_S	p $\left(\frac{\text{kJ}}{\text{mol nm}^3}\right)$	ρ $\left(\frac{\text{u}}{\text{nm}^3}\right)$	D $\left(10^{-3}\ \frac{\text{nm}^2}{\text{ps}}\right)$	ε_S
NVT	0.907	473.7	2.6	22.7	−0.035	452.1	4.2	24.6
NPT	0.048	473.1	2.4	19.8	0.088	452.5	4.4	23.8
Expt.	0.061	473.7 (Ref. 29)	2.4 (Ref. 65)	32.6 (Ref. 33)	0.061	456.4[a]	3.8 (Ref. 65)	27.6 (Ref. 54)

[a]Interpolated from values (Ref. 29) at 323 K and at 333 K.

found for united atom models. The diffusion constant increases with increasing temperature as shown in Table VIII. This is in agreement with experiment, but the rise is too steep compared to experiment.

The value of the shear viscosity obtained for model B3 was 236 $\text{kJ mol}^{-1}\,\text{nm}^{-3}\,\text{ps}$, which is lower than the experimental value[57] of 326 $\text{kJ mol}^{-1}\,\text{nm}^{-3}\,\text{ps}$ at 298 K. Mountain[55] and Wheeler and Rowley[27] both calculated the viscosity of model L1 and obtained values that were higher than the experimental values, 391 $\text{kJ mol}^{-1}\,\text{nm}^{-3}\,\text{ps}$ and 346.65 $\text{kJ mol}^{-1}\,\text{nm}^{-3}\,\text{ps}$, respectively.

B. Dielectric properties

The dielectric constant is smaller than the experimental value for all models, with model B3 having the highest and model GR96 the lowest value. The underestimation of the dielectric constant is most likely due to the neglect of the electronic polarizability. With increasing temperature (see table VIII) the dielectric constant of model B3 increases, although the experimental value decreases. However, the simulated increase of ε_S with temperature may not be significant: the values obtained from the 1900 ps trajectories have an estimated error of about 7%. This size of convergence error for ε_S was found when using 1900 ps averaging in a recent MD simulation study of liquid water extending over several nanoseconds (A. Glättli, private communication). Secondly, the contributions of the electronic and orientational polarization to ε_S may be different at different temperatures. Since the former contributions are neglected in our model, the temperature dependence of ε_S may be incorrectly modeled.

The differences between the simulation at constant pressure and the one at constant volume decreases with rising temperature, though the result from the constant pressure run is still lower than from the one at constant volume. The value for model H1 is lower than those of Richardi *et al.*[58] and of Fonseca and Ladanyi,[59] who obtained 25.3 and 24, respectively. The value determined for model L1 is lower than the value given by Mountain,[55] 22. The Debye relaxation time is much lower than the experimental value for all models, with model L1 coming closest to it.

C. Thermodynamic properties

The calculated isothermal compressibility for model B3 is $1.6\times10^{-3}\,\text{kJ}^{-1}\,\text{mol nm}^3$, lower than the experimental value[33] of $2.0\times10^{-3}\,\text{kJ}^{-1}\,\text{mol nm}^3$. A too low compressibility shows that the liquid is too resistant to compression when put under pressure. This may be a consequence of the chosen representation for the nonbonded interaction. The r^{12} term in the Lennard-Jones function is known to cause too sharp an increase of energy at small atom–atom distances.[40] The calculated heat capacity is 95.44 $\text{J mol}^{-1}\,\text{K}^{-1}$ to be compared to the experimental value[60] of 81.47 $\text{J mol}^{-1}\,\text{K}^{-1}$.

Two simulations at a higher temperature (328 K), one with constant pressure and one with constant volume were performed. The simulation at constant volume is not at the experimental density but at the density that gives a pressure close to 1 atm. The calculated permittivity is not distorted by pressure effects. The results are shown in Table VIII. From the simulations at constant pressure the thermal expansion coefficient α can be calculated via Eq. (13). In this way an α of $1.50\times10^{-3}\,\text{K}^{-1}$ was obtained, which is close to the experimental value[33] of $1.49\times10^{-3}\,\text{K}^{-1}$.

D. Free energy

Both the excess Helmholtz energy and the hydration free energy of model B3 are close to the experimental value. The excess Helmholtz energy was found to be equal to 17.0 kJ/mol. This may be compared to an experimental value, calculated by Eq. (18) of 17.8 kJ/mol. The hydration free energy was calculated as −21.4 kJ/mol which agrees very well with the experimental value of −21.4 kJ/mol.[61]

E. Mixing with water

The distribution of methanol and water molecules in the mixtures is homogeneous, as is illustrated in Fig. 1. For $x_{\text{MeOH}}=0.5$, the first peak in the oxygen–oxygen radial distribution function for water–methanol pairs is as large as the ones for the water–water and methanol–methanol pairs.

The results for the mixing enthalpy, calculated by Eq. (16), are shown in Fig. 2 together with the experimental values.[62] A negative mixing enthalpy was obtained over the whole range of mixtures. The experimental values are slightly more negative and the largest deviation from ideal mixing behavior occurs at a methanol fraction near 0.3, whereas the largest deviation from ideality for B3 methanol mixed with SPC water occurs at $x_{\text{MeOH}}=0.5$.

Ferrario *et al.*[24] reported an excess enthalpy of mixing of −1.3 kJ/mol for H1 methanol together with TIP4P water[63] (NVT) which they compared to an experimental value of −0.9 kJ/mol. Stouten[23] obtained a value of −0.767 kJ/mol for an equimolar mixture of the flexible OM2 methanol

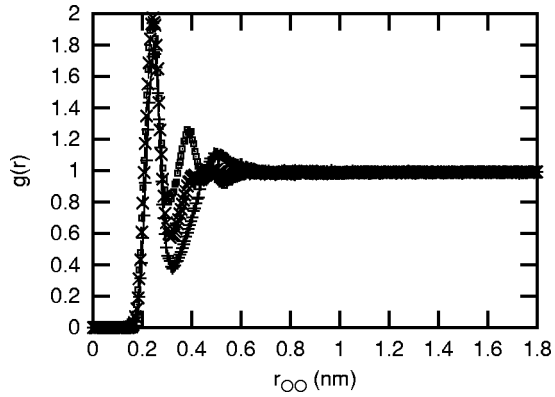

FIG. 1. Oxygen–oxygen radial distribution functions for a $x_{MeOH}=0.5$ mixture of methanol and water: methanol–methanol pairs: +, solid line; methanol–water pairs: ×, dashed line; water–water pairs: □, short-dashed line.

model and SPC water (NPT), compared with the experimental value of −0.8 kJ/mol at 297.21 K. Freitas[25] performed Monte Carlo simulations of J2 methanol with TIP4P water for methanol mole fractions equal to 0.10, 0.25, 0.50, and 0.75 in the NVT and NPT ensembles. The values at NPT were systematically too high (e.g., $\Delta H_{mix}=-0.574$ kJ/mol at $x_{MeOH}=0.25$). The enthalpies of mixing at NVT using the experimental densities were in better agreement with the experimental data.

The densities of the methanol–water mixtures are presented in Fig. 3 together with the experimental values.[57] The calculated densities agree closely with experiment over the whole range of mixtures, except close to $x_{MeOH}=0$, where the too low density of SPC water compared to experiment plays a bigger role.

For the J2 methanol model together with TIP4P water Freitas[25] found that the simulated densities are smaller than the experimental values and the error increased with increasing methanol concentration. For a methanol mole fraction of $x_{MeOH}=0.50$ a density of 524 u nm^{-3} was reported, to be compared to the B3/SPC value of 527 u nm^{-3} and to the experimental value[64] of 531 u nm^{-3}. Stouten[23] obtained a density of 529 u nm^{-3} at 297.21 K. Laaksonen *et al.*[26] got a density of 533 u nm^{-3} at 300 K for a mixture of Haughney's methanol model and SPC.

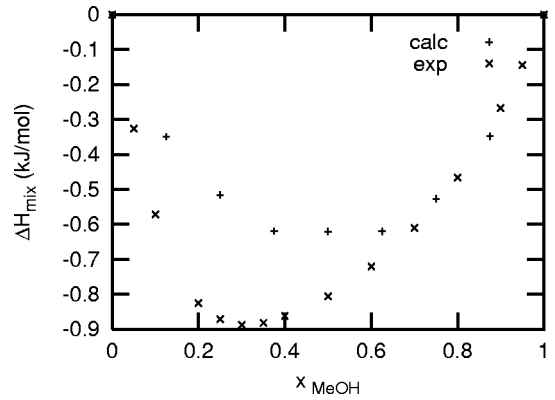

FIG. 2. The mixing enthalpy at 298 K is calculated with Eq. (16). The experimental values are taken from Landolt–Börnstein (Ref. 62).

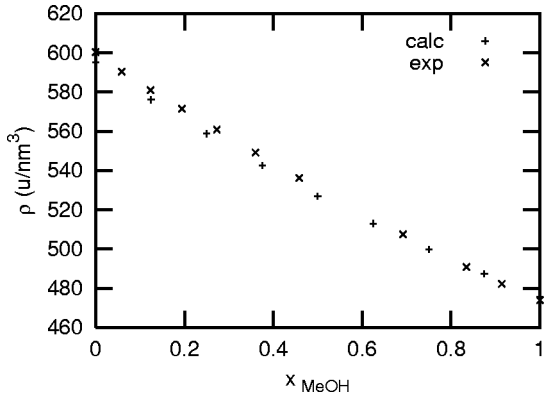

FIG. 3. Density of the mixtures at 298 K. The experimental values are taken from Mikhail (Ref. 57).

V. CONCLUSION

We have presented a methanol model and compared its performance for a wide range of properties to models found in the literature. To achieve this goal each model has been simulated under the same conditions for long simulation times. Our model B3 is shown to be in overall agreement with experiment and to be competitive concerning the reproduction of a variety of experimental quantities with reference models from the literature. The initial aim of getting a model that combines well with SPC water and that has a dielectric permittivity close to the experimental value is only partly fulfilled. The B3 methanol model interacts well with SPC water over the whole range of mole fractions and also reproduces well the hydration free energy. It proved not possible to reproduce the experimental dielectric permittivity with a simple 3 site rigid model for methanol. By systematically varying a wide range of model parameters we have been able to demonstrate the sensitivity of various simulated properties of liquids to the underlying model. This work clearly demonstrates that basic properties such as the density and pressure can be reproduced with a wide range of parameters and that the correct density and pressure is a necessary but not sufficient condition for a good model. The work also highlights the sensitivity of those models to the precise simulation conditions and the need for the incorporation of polarizability if dielectric properties are to be correctly reproduced.

[1] H. Kovacs, A. E. Mark, J. Johansson, and W. F. van Gunsteren, J. Mol. Biol. **247**, 808 (1995).
[2] P. E. Smith and B. M. Pettitt, J. Phys. Chem. **98**, 9700 (1994).
[3] A. M. Klibanov, TIBS **14**, 141 (1989).
[4] M. Norin, F. Haeffner, K. Hult, and O. Edholm, Biophys. J. **67**, 548 (1994).
[5] D. S. Hartsough and K. M. Merz, Jr., J. Am. Chem. Soc. **115**, 6529 (1993).
[6] C. L. Brooks III, M. Karplus, and B. M. Pettitt, Adv. Chem. Phys. **71**, 1 (1988).
[7] H. J. C. Berendsen, J. P. M. Postma, W. F. van Gunsteren, and J. Hermans, in *Intermolecular Forces*, edited by B. Pullman (Reidel, Dordrecht, 1981), pp. 331–342.
[8] W. F. van Gunsteren, S. R. Billeter, A. A. Eising, P. H. Hünenberger, P. Krüger, A. E. Mark, W. R. P. Scott, and I. G. Tironi, *Biomolecular Simulation: The GROMOS96 Manual and User Guide* (vdf Hochschulverlag, ETH Zürich, Switzerland, 1996).
[9] W. L. Jorgensen, J. Phys. Chem. **90**, 1276 (1986).

[10] M. Haughney, M. Ferrario, and I. R. McDonald, Mol. Phys. **58**, 849 (1986).
[11] M. Haughney, M. Ferrario, and I. R. McDonald, J. Phys. Chem. **91**, 4934 (1987).
[12] M. E. van Leeuwen and B. Smit, J. Phys. Chem. **99**, 1831 (1995).
[13] W. L. Jorgensen, J. Am. Chem. Soc. **103**, 341 (1981).
[14] G. Ciccotti, M. Ferrario, and J. P. Ryckaert, Mol. Phys. **47**, 1253 (1982).
[15] P. F. W. Stouten, Ph.D. thesis, Rijksuniversiteit, Utrecht, The Netherlands, 1989.
[16] A. Z. Panagiotopoulus, Mol. Phys. **61**, 813 (1987).
[17] M. Mezei, Mol. Simul. **9**, 257 (1992).
[18] G. Bolis, G. Corongiu, and E. Clementi, Chem. Phys. Lett. **86**, (1982).
[19] W. L. Jorgensen and J. D. Madura, J. Am. Chem. Soc. **105**, 1407 (1983).
[20] S. Okazaki, K. Nakanishi, and H. Touhara, J. Chem. Phys. **78**, 454 (1983).
[21] G. Pálinkás, I. Bakó, and K. Heinzinger, Mol. Phys. **73**, 897 (1991).
[22] G. Pálinkás, E. Hawlicka, and K. Heinzinger, Chem. Phys. **158**, 65 (1991).
[23] P. F. W. Stouten and J. Kroon, Mol. Simul. **5**, 175 (1990).
[24] M. Ferrario, M. Haughney, I. R. McDonald, and M. L. Klein, J. Chem. Phys. **93**, 5156 (1990).
[25] L. C. G. Freitas, J. Mol. Struct.: THEOCHEM **282**, 151 (1993).
[26] A. Laaksonen, P. G. Kusalik, and I. M. Svishchev, J. Phys. Chem. **101**, 5910 (1997).
[27] D. R. Wheeler and R. L. Rowley, Mol. Phys. **94**, 555 (1998).
[28] J.-P. Ryckaert, G. Ciccotti, and H. J. C. Berendsen, J. Comput. Chem. **23**, 327 (1977).
[29] *American Institute of Physics Handbook*, 3rd ed., edited by D. E. Gray (McGraw-Hill, New York, 1972).
[30] H. J. C. Berendsen, J. P. M. Postma, W. F. van Gunsteren, A. DiNola, and J. R. Haak, J. Chem. Phys. **81**, 3684 (1984).
[31] M. Neumann, J. Chem. Phys. **82**, 5663 (1985).
[32] I. G. Tironi, R. Sperb, P. E. Smith, and W. F. van Gunsteren, J. Chem. Phys. **102**, 6199 (1995).
[33] *Handbook of Chemistry and Physics*, 56th ed., edited by R. C. West (CRC, Boca Raton, 1976).
[34] J. P. M. Postma, Ph.D. thesis, Rijksuniversiteit, Groningen, The Netherlands, 1985.
[35] M. D. Harmony *et al.*, J. Phys. Chem. Ref. Data **8**, 619 (1979).
[36] M. Lauterbach, Ph.D. thesis, Université Louis Pasteur, Strasbourg, France, 1997.
[37] W. F. van Gunsteren and H. J. C. Berendsen, GROningen MOlecular Simulation (GROMOS) library manual, Biomos, Nijenborgh 4, 9747 AG Groningen, The Netherlands, 1987.
[38] A. L. McClellan, *Tables of Experimental Dipole Moments* (Rahara Enterprises, El Cerrito, CA, 1989), Vol. 3.
[39] W. F. van Gunsteren, X. Daura, and A. E. Mark, Encyclopedia of Computational Chemistry **2**, 1211 (1998).
[40] I. G. Tironi and W. F. van Gunsteren, Mol. Phys. **83**, 381 (1994).
[41] M. P. Allen and D. J. Tildesley, *Computer Simulation of Liquids* (Clarendon, Oxford, 1987).
[42] M. Neumann, Mol. Phys. **50**, 841 (1983).
[43] K. A. Motakabbir and M. Berkowitz, J. Phys. Chem. **94**, 8359 (1990).
[44] G. Herzberg, *Molecular Spectra and Molecular Structure, II. Infrared and Raman Spectra of Polyatomic Molecules* (van Nostrand, Princeton, NJ, 1960).
[45] E. B. J. Wilson, Chem. Rev. **27**, 17 (1940).
[46] G. Wedler, *Lehrbuch der Physikalischen Chemie* (VCH, Weinheim, Germany, 1987).
[47] T. C. Beutler *et al.*, Chem. Phys. Lett. **222**, 529 (1994).
[48] M. Zacharias, T. P. Straatsma, and J. A. McCammon, J. Chem. Phys. **100**, 9025 (1994).
[49] X. Daura *et al.*, J. Am. Chem. Soc. **118**, 6285 (1996).
[50] J. Hermans, A. Pathiaseril, and A. Anderson, J. Am. Chem. Soc. **110**, 5982 (1988).
[51] H. J. C. Berendsen, J. R. Grigera, and T. P. Straatsma, J. Phys. Chem. **91**, 6269 (1987).
[52] P. E. Smith and W. F. van Gunsteren, J. Chem. Phys. **100**, 3169 (1994).
[53] H. Fröhlich, *Theory of Dielectrics, Dielectric Constant and Dielectric Loss*, Monographs on the Physics and Chemistry of Materials, 2nd ed. (Clarendon, Oxford, 1958).
[54] G. H. Barbenza, J. Chim. Phys. Phys.-Chim. Biol. **65**, 906 (1968).
[55] R. D. Mountain, Mol. Phys. **94**, 435 (1998).
[56] N. Asahi and Y. Nakamura, J. Chem. Phys. **109**, 9879 (1998).
[57] S. Z. Mikhail and W. R. Kimel, J. Chem. Eng. Data **6**, 533 (1961).
[58] J. Richardi, C. Millot, and P. H. Fries, J. Chem. Phys. **110**, 1138 (1999).
[59] T. Fonseca and B. M. Ladanyi, J. Chem. Phys. **93**, 8148 (1990).
[60] J. A. Riddick, W. B. Bunger, and T. K. Sakano, *Organic Solvents: Physical Properties and Methods of Purification* (Wiley, New York, 1986).
[61] S. Cabani, P. Gianni, V. Mollica, and L. Lepori, J. Solution Chem. **10**, 563 (1981).
[62] G. Beggerow, *Landolt–Börnstein: Heats of Mixing and Solution*, Vol. IV/2 of New Series (Springer, Berlin, 1976).
[63] W. L. Jorgensen *et al.* J. Chem. Phys. **79**, 926 (1983).
[64] G. Clifford and J. A. Campbell, J. Am. Chem. Soc. **673**, 5449 (1951).
[65] R. L. Hurle and L. A. Woolf, Aust. J. Chem. **33**, 1947 (1980).